UM-P-89/90

COMPUTER-SIMULATED IMAGES OF ICOSAHEDRAL, PENTAGONAL AND DECAGONAL CLUSTERS OF ATOMS

by

Peng JuLin and L.A. Bursill*

School of Physics
University of Melbourne
Parkville, Victoria 3052
Australia

* correspondence

1. Introduction

Many authors have published high-resolution electron microscope (HREM) images of icosahedral and decagonal alloys (see for example some collected papers on aperiodic and quasicrystalline alloys [1,2]). However it has been disappointing that analysis of such images of aperiodic alloy structures has failed to establish definitive structural information. The images often reveal interesting arrays of black and white spots (see for example Fig. 1a, taken from a sample of $A\ell_6Mn$ [3]). Pentagonal and decagonal rings of white (or black) intensity occur which map readily onto two-dimensional Penrose tiling patters [3,4]. Agreement between image and tiling patterns is not fortuitous, the images of course are themselves decorated tilings possessing local pentagonal and decagonal symmetries, whereas the symmetry of the optical transform of the images or the power spectra must be decagonal [5]. To deduce the three-dimensional quasi-crystalline structure is a typical non-trivial inversion problem for diffraction theory [5]. In the following we investigate, by computer-simulation, HREM images for a set of icosahedral and decagonal clusters, containing 50-400 atoms. The aim of this work was to probe the model-sensitiveness of HREM images to such aperiodic structures, given optimized electron optical imaging parameters.

This work has led to a new experimental study of both crystalline and quasi-crystalline alloys of Aℓ(Si)Mn [6]. Thus carefully-chosen electron optical conditions were established by computer simulation then used to obtain high quality experimental images which could be analyzed in a meaningful way.

For the present volume of SYMMETRY it seemed appropriate to publish a variety of the computer-simulated images, which are of interest for aesthetic as well as scientific value.

Small icosahedral clusters of atoms have intrinsic scientific interest in

terms of the energetics and stablity of ultra-fine particles.

The catalytic activity of such small clusters of atoms makes them interesting too, from the point of view of applied chemistry and chemical engineering.

In section (#2) we introduce briefly the subject of ultra-fine metal cluster structure research, placing it in context with respect to the subject of quasi-crystallinity; then follows a survey of structural models investigated (#3); a description of the computer-simulation technique for image analysis (#4); the results of the computer-simulations testing model sensitiveness of the HREM images (#5) and finally (#6) our conclusions.

2. Ultra-fine Atomic Clusters and Quasi-crystals

The study of the symmetry and structure of clusters of 12, 13, 55 - up to several 100's of atoms lies at the core of understanding the relative stability of icosahedral alloys, both crystalline and quasi-crystalline, as well as of glassy metals. Frank [7] considered an icosahedral cluster of 12 atoms about a central sphere as energetically preferable to cubic or hexagonal close-packed coordination spheres (e.g. cubactohedral, etc.), at least for simple Lennard-Jones pair potentials. He used this argument to explain the remarkable degree of supercooling possible in simple liquid metals due to the abundance of icosahedral clusters. It was a modern study of this problem which led Steinhardt into the subject of quasicrystals [8]. Frank's work later extended to the glass/crystalline transition as a supercooled liquid approaches a Frank-Kasper phase [9], introducing the concept of a disordered disclination network [10]. Extended icosahedral correlations were also proposed in small "amorphon" cluster models of the structure of metallic glasses [11]. Pauling [12] provided a beautifully clear statement of the transition from clusters having icosahedral symmetry in the liquid state into complex crystalline alloy phases, see especially his Fig. 11-14 [12].

The structures of metallic particles used as catalysts lie somewhere between those of translationally periodic crystalline arrangements and the aperiodic aggregates proposed for glasses. Hoare [11] has described a range of coordination polyhedra, often invoking the concept of multiple-internal-twinning; forerunner of the controversy between proponents of the reality of Penrose tiling patterns [13] versus Pauling's claim for multiply-twinned crystalline phases [14]. Such multiply-twinned particles may grow from a nucleus of four atoms in a tetrahedral close-packed arrangement, onto which additional atoms occupy the centres of each face, producing very stable clusters of 7 or 13 atoms, which become the precursors of the pentagonal bipyramid or icosahedron respectively [11]. These shapes may be maintained by the addition of shells of atoms [15] which for small clusters, are thought to be relatively more stable than a cluster of the same number of atoms having a fcc or hcp structure. It would seem likely that extended arrays of pentagonal bipyramidally coordinated clusters should lead naturally to decagonal quasi-crystalline alloys, in the same way that icosahedral or rhombic triacontahedral units should lead to icosahedrally-symmetric quasi-crystals [16]. In addition to decorations of two or three-dimensional Penrose tilings [17], it is possible to conceive of hierarchical packings of icosahedral units [18] or essentially randomly positoned icosahedral units [19] which are cemented together by Aℓ or Mn atoms; in the latter case a large proportion of the atoms have bond-orientational order (which may be perfect in a Penrose tiling) but there are also a significant proportion of "fill in" atoms which are not necessarily part of an icosahedral cluster.

3. Description of Some Icosahedral and Pentagonal Test Objects.

A cartesian set of axes was used for the atomic coordinates and cell edges. These are shown schematically in Fig. 2, where the relationship to a six-axial system is indicated. Note that the twelve vertices of a regular

icosahedron may be decomposed into sets of vertices of three orthogonal golden rectangles, shown in Fig. 2. Thus $g_1 = (\tau, \bar{1}, 0)$, $g_2 = (\tau, 1, 0)$, $g_3 = (0, \tau, 1)$, $g_4 = (\bar{1}, 0, \tau)$, $g_5 = (0, \tau, 1)$, $g_6 = (1, 0\ \tau)$. Fig. 3 shows pentagonal rings containing five elementary units. These may stack along a five-fold projection axis with the second and succeeding levels either eclipsed (Fig. 3a) or staggered (Fig. 3b) forming columns of pentagonal prisms (Fig. 3c) or pentagonal antiprisms (Fig. 3d) as indicated. Capping antiprisms top and bottom (Fig. 3e) gives rise to pentagonal clusters consisting of face-shared pairs of truncated icosahedra (Fig. 3f). Such stuctural units may be used to decorate two-dimensional Penrose tilings, as shown in Figs. 4a, b, c. Successive layers may be added, to produce hexagonal prisms (Fig. 4d), pentagonal antiprisms (Fig. 4e) or coherent mixtures of prisms and antiprisms (Fig. 4f). The above models (Figs. 3, 4) all posses a single five-fold or $1\bar{0}$ axis.

In Fig. 5 a series of structural models is developed, starting with a pentagonal ring of icosahedra in Fig. 5a. Successive icosahedra may be added in corner-shared (Fig. 5b) or edge-shared fashion (Figs. 5c). The latter forms a much denser cluster (Fig. 5d), possessing $1\bar{0}$ point symmetry. Figs. 5 e, f, g show alternative ways of filling the central position within pentagons, designed to allow changes in the relative occupancies of pentagonal centres to be compared.

These same modelling principles may be extended for decorated Penrose tilings, as shown in Figs. 6a, b, c. Again any number of stacking variants may be invoked along the unique 5-fold or $1\bar{0}$ projection axis, illustrated by Figs. 6d-h. The periodicity along the projection axes may be chosen to model various decagonal phases [20]. This set of models was designed to vary the relative amounts of edge- and corner-sharing of pentagonal prisms, antiprisms or icosahedra. Thus we were able to investigate the model sensitivity of the computed images to varying

occupancies of ring or centering positions along the projection axis.

Hiraga [18] proposed a three-dimensional structure for an icosahedral phase (so-called "hierarchical model") in which twelve unit icosahedra (edge a_0; see Fig. 7a) aggregate by edge-sharing to form a larger icosahedron of edge length $a_1 = (2 + 1/\tau)a_0$ (Fig. 7c) where τ is the golden mean. Similarly, further generations of icosahedral clusters may be envisaged (Fig. 7c) with edge-length $a_n = (2 + 1/\tau)\, a_0$. The fundamental icosahedral units may be centred or non-centred (Figs. 7a, b). It is worth noting that it is necessary to introduce a further tesselation of the central icosahedron for each hierarchical generation (Fig. 7c), in order to avoid leaving voids in this model. There are also some unrealistically short interatomic distances (a_0/τ) which would have to be avoided in a real structure. However, it was interesting to compare computer simulations for these giant molecular clusters with those for three-dimensional Penrose tilings.

Unit rhombic triacontahedra were constructed, following Mackay [16], out of 10 oblate and 10 prolate rhombohedra (α = 63.43° and 116.57° respectively, Figs. 8 a, b)). A perpective view is given as Fig. 8c. A second generation cluster was then constructed, shown projected along a five-fold axis in Fig. 8d. Note that only the external facets form an object with true icosahedral symmetry. Permutations of the basic rhombohedral units would readily lower the true symmetry of the cluster to pseudoicosahedral for a real structure. We have chosen a symmetrical model (Fig. 8d) for purposes of computer-simulations.

All of the models used in simulations are summarized in Table 1, when a shorthand symbol for each distinct type may be found. Note that in the simulations the unit interatomic distance was chosen as a_0 = 2.8Å, as appropriate for Aℓ-Aℓ, for example. For the triacontahedral model the unit rhombohedra had edge length a_R = 4.6 Å.

4. Computer-Simulation Technique

The calculations were based on the physical optics approach to electron diffraction and imaging due to Cowley and Moodie [21] using the multislice technique introduced by Goodman and Moodie [22]. All of the non-linear N-beam dynamical scattering, as well as lens aberrations and Fresnel propagation effects in the objective lens of a HREM instrument were included. Periodic continuation methods, as developed for atomic resolution images [23, 24, 25] were obtained using MUM software (Melbourne University Multislice). This allows HREM images of finite aperiodic objects to be simulated reliably. Thus diffuse scattering, due to finite size effects, as well as internal defects in packing, may be readily included in the calculations. The atomic clusters (described above) were placed at the centre of a large pseudocrystalline unit cell (dimensions are given in Table1), when there was minimum overlap of waves scattered by adjacent clusters. The image of one such unit cell then exhibits contrast virtually identical to that of an isolated cluster. The techniques were first applied to small icosahedral clusters of gold atoms by Barry, Bursill and Sanders [26]. The present report is restricted to 5- or $\bar{1}0$-fold projection axes of icosahedral and decagonal clusters of atoms. The electron optical parameters refer to a JEOL-2000EX instrument with spherical aberration coefficient C_s = 0.9 mm and chromatic aberration defocus spread 50 Å. Through-focal series of images were obtained for the useful range of experimental values typical for this instrument, ie. - 1000 ≤ Δf Å ≤ 1400. Note that the so-called Scherzer optimum focus condition occurs for Δf = -600 Å. The affective resolution of the image simulations was limited to 2.3 Å, the value expected for interpretable structure images for the JEOL-2000EX instrument [27].

5, Results

(a) <u>Small Clusters</u>: Fig. 9 gives a matrix of computed images for 11

different clusters as a function of objective lens defocus (- 1000 ≤ Δf Å ≤ 400). Note there are interesting changes of contrast with both objective lens defocus, and structural model. As well as changes in internal detail, the apparent shape changes significantly with defocus. Fresnel fringe detail extends outwards in the vicinity of a cluster, which effect becomes dominant for Δf values far from the Scherzer optimum image condition (Δf = - 600 Å). Fresnel effects also superpose on fine detail within the cluster, since the latter contain surface facets (cluster/vacuum interfaces) which are characteristic of the cluster and may produce significant phase contrast in the images. These optical details do not directly represent atomic detail of course, although for some clusters it may provide a distinctive "fingerprint" image. Note in Fig. 9 (models C-F) that pentagonal rings of 5 white spots are relatively stable for -600 ≤ Δf Å ≤ -300, although the pentagons change slightly in edge dimension. Black spot contrast within the cluster does not necessarily represent the projected potential or atomic charge density in the cluster. Similarly, white spots do not necessarily represent relatively empty tunnels through the cluster; rather, they represent sites at the centre of pentagonal rings. The intensity and size of such white spots may vary with the projected occupancy of such sites. In general, at Scherzer defocus (Δf = - 600Å), the higher the projected atomic density the larger and darker the black spots or the smaller and weaker are the light spots. Thus these cluster images are structure model sensitive but it may not be a trivial matter to solve the inversion problem, i.e. convert image intensity into atomic density or projected potential. However, corner-shared pentagonal rings (A) should be distinguishable from clusters containing face-sharing pentagonal prisms (B) or edge-sharing icosahedral structural units (A). In particular the latter shows just-resolved rings of 10 black or white spots, depending on defocus.

The first generation icosahedral clusters, whether centred (K) or non-

centred (L) show relatively well-resolved 10-rings, the ring diameter varies with defocus. For the Scherzer condition the ring diameter of 7.8 Å is consistent with the icosahedral ring diameter. The triacontahedral cluster (J) behaves in a distinct fashion, compared with the first general hierarchial cluster (K). The former gives a 13.2 Å diameter 10-ring of black spots (at Scherzer), which undergoes a contrast reversal to 10- and 5-rings of white spots as defocus varies away from Scherzer. As well we see a changing diameter for the 10-ring of white spots. Clearly, if any structural information is to be available directly from the image then it is essential to identify the Scherzer optimum defocus condition.

(b) Two-dimensional Penrose Tiling Models: A matrix of images for 7 two-dimensional Penrose tilings are given in Fig. 10 as a function of objective lens defocus ($-1000 \leq \Delta f$ Å ≤ 400). As for Fig. 9 the images are model sensitive to a significant extent, at the Scherzer optimum defocus condition for example ($\Delta f = -600$ Å). When the through-focal-series are compared even greater discrimination between models is readily apparent, surpassing that exhibited by the smaller clusters. The model Q shows a remarkable similarity to an experimental image (Fig.1). Individual pentagonal prismatic or antiprismatic columns may be identified as a white spot and larger dark spots correspond to edge-shared icosahedral units, for $\Delta f = -600$Å. All of the images may be identified as decorated two-dimensional Penrose tilings, at least in the interior away from edge effects.

It is interesting to ask if the degree of model-sensitiveness of the images may be increased by availability of higher instrumental resolution. Fig. 11 shows a through focus/through resolution matrix of images for model (Q). Briefly we conclude that fine detail certainly increases with higher resolution, for all defocus settings. However most of this increased detail is of little use, as it is not simply related to the projected atomic positions in the

corresponding cluster (e.g. Fig.4b). However, some aesthetically pleasing results were obtained.

(c) **Second-generation hierarchical model**: Complete through-focal series of images for the centred and non-centred hierarchical models are illustrated in Figs. 12 a,b (-1000 $\leq \Delta$d Å $\leq$ 1400). Comparison of the two models for any given defocus, e.g. Δf = - 600 Å will reveal quite distinct images, even for such a relatively small change of structure. However, for 2.3 Å resolution there is virtually no direct structural information, in terms of one-for-one relationship with projected charge density. Furthermore, increases in instrumental resolution (at 200 kV) are likely to make interpretation more, rather than less, difficult. Comparison of hierarchical with rhombic triacontahedral clusters is however quite revealing.

(d) **Rhombic-triacontahedral clusters**: A through-focal series (- 1000 $\leq \Delta$f Å $\leq$ 400) is given for model J in Fig. 12c. All of the images are quite distinct from those of the hierarchical model (Fig. 12 a,b) but ressemble those of the two-dimensional Penrose tilings (Fig. 10). The image at Scherzer (Δf = - 600Å) most closely ressembles the structure, but the effective thickness of the cluster was only 26 Å, which is really almost two-dimensional. Six interlocking decagonal rings of black spots may be found for Δf = - 600 Å or - 500 Å whereas six interlocking rings of white spots are found for Δf = - 1000 Å, - 900 Å, - 400 Å, - 100 Å and 100 Å. This set of images are strictly pseudopentagonal due to our choice of occupancies in the calculation. Departures from 5 fold symmetry become more apparent for specific Δf values.

6. Conclusion

The computer simulations above have allowed us to explore the

limitations of HREM image analysis for structure determination of quasi-crystalline clusters or even local structural elements in extended aperiodic objects. Clearly, there is a very significant degree of model sensitiveness avilable, in the sense that the image may provide a fingerprint for certain structural elements, provided electron optical parameters such as specimen thickness and objective lens defocus have been determined. Equally clear, however, is the fact that direct inversion from image to structure is not a realistic possibility. Whereas many possible structures may be eliminated it may not be possible to arrive at unique structural solutions.

Based on the above experience it occurred to us that a reasonable procedure would be to record experimental images of known complex icosahedral ailoys, in the crystalline phase, then use the computer-simulations to identify "fingerprint" imaging conditions whereby certain structural elements could be relaibly identified in images of aperiuodic quasi-crystalline or amorphous specimens. This principle has been used by Mr. Song in subsequent work [6].

From the present results it is worth noting that the experimental image (Fig. 1a) could be reproduced to a large extent (Fig. 1b) by cluster model Q (Table 1) but some details were not reproduced. That image suffered from the experimental uncertainty that it could not be proven à priori whether the specimen ($A\ell_6Mn$) was icosahedral or decagonal phase, nor were the thickness of defocus conditions established. In the subsequent work on Aℓ(Si)Mn crystalline and icosahedral alloys strenuous efforts have been made to correct these limitations [6].

Acknowledgements

This work was supported by the Australian Research Council. Peng JuLin is grateful for the award of a National Research Fellowship.

References

[1] D.Gratias and L.Michel (Eds.) "International Workshop on Aperiodic Crystals", Les Houches, March 1986, Published in J. de Physique Colloqui C3, supplement au No.7 (1986).

[2] P.J.Steinhardt and S.Ostlund (Eds.) "The Physics of Quasicrystals", World Scientific, Singapore (1987).

[3] L.A.Bursill and Peng JuLin, Nature 316, 50 (1985).

[4] P.Guyot and M.Audier, J.Micros. S10, 575 (1985) also Phil.Mag. B53, 143-51 (1986).

[5] J.M.Cowley "Diffraction Physics" 2nd Ed. North-Holland (1981).

[6] Guang Li Song, Ph.D. thesis, University of Melbourne, in prep. (1989).

[7] F.C.Frank, Proc.Roy.Soc. (Lond.) A215, 43 (1952).

[8] D.Levine and P.J.Steinhardt, Phys.Rev.Letts. 53, 2477 (1984).

[9] F.C.Frank and J.S.Kaspar, Acta Crystallogr. 11, 184 (1958) and ibid 12, 483 (1959).

[10] D.R.Nelson, Phys.Rev.Letts. 50, 982 (1983) and Phys. Rev. B28, 5515 (1983).

[11] M.R.Hoare, Ann. N.Y. Acad. Sci. 279, 186 (1976).

[12] L.Pauling "The Nature of the Chemical Bond", 3rd Ed. Cornell Univ. Press (1960), p428.

[13] Letters to the Editor, Nature 319, 102 (1986).

[14] L.Pauling, Phys.Rev.Letts. 589, 365 (1987).

[15] A.L.Mackay, Acta Crystallogr. 15, 916 (1962).

[16] A.L.Mackay, Physica 114A, 609 (1982).

[17] V.Elser and C.J.Henley, Phys. Rev. Letts. 55, 2883 (1985).

[18] K.Hiraga, M.Hirabayashi, A. Inoue and T.Masumoto, Sci. Rep. Res. Inst. Tohoku Univ., A32, 309 (1985).

[19] D.Schechtman and I.A.Blech, Metall. Trans. 16A, 1005 (1985).

[20] K.K.Fung, C.Y.Yang, Y.Q.Zhou, W.S.Zhan, and B.G.Shen, Phys.Rev.Letts. 56, 2060 (1986).

[21] J.M.Cowley and A.F.Moodie, Proc. Phys. Soc. (Lond.) 76, 378 (1960).

[22] P.Goodman and A.F.Moodie, Acta Crystallogr. A 30, 280 (1974).

[23] D.S.Maclagen, L.A.Bursill and A.E.C.Spargo, Philos.Mag. 35 , 757 (1977).

[24] A.R.Wilson, L.A.Bursill and A.E.C.Spargo, Optik 52, 3313 (1978/79).

[25] Peng JuLin and L.A.Bursill, Optik 81, 167 (1989).

[26] J.C.Barry, L.A.Bursill and J.V.Sanders, Austral.J.Phys. 38, 437 (1985).

[27] L.A.Bursill, J.C.Barry and J.L.Hutchinson, Optik 65, 251 (1983).

Figure Captions

Figure 1a: HREM image of Al_6Mn quasi-crystalline alloy specimen; this area shows a localized pseudo-five fold symmetry axis.

Figure 1b: Computer-simulated image for cluster model PQ (See Fig. 6b below). Large white spots match Fig. 1a but fine detail does not.

Figure 2: Relationship between six-axial basis set $\underline{g}_i$ (i = 1....6) and Cartesian axes X, Y, Z.

Figure 3: (a) Pentagonal cluster (eclipsed layers) giving rise to (b) pentagonal prismatic columns along 5-fold axis. Capping top and bottom (c) gives rise to face-shared truncated icosahedra (f).

(c) Pentagonal cluster (staggered layers) giving rise to

(d) pentagonal antiprismatic columns along 5-fold axis.

Figure 4: (a) Two-dimensional Penrose tiling (eclipsed stacking) giving rise to (d) pentagonal prismatic columns. (b) Two-dimentional cluster (staggered stacking) giving rise to

(e) pentagonal antiprisms. (c) Shows third- and fourth-layers of a cluster containing a mixture of pentagonal prisms (a) and antiprisms (c) with sequence given in (f).

Figure 5: (a) Pentagonal cluster of five icosahedra surrounding a central stellated icosahedron. (b) to (g) show five different ways of extending (a) along a unique 5-fold axis giving rise to different occupancies at sites shown in projection shown in

(a); (c) shows cluster of ten icosahedra surrounding a central tesselated icosahedron; (d) shows nature of edge-sharing of icosahedra in (c).

Figure 6: (a)(b)(c) Extended two-dimensional Penrose tilings of icosahedra (or truncated icosahedra) which may be stacked according to (d)(e)(f)(g) or (h) to produce a variety of atomic densities viewed along a 5-fold (or $1\bar{0}$) projection axis.

Figure 7: Filled (a) or empty (b) icosahedral units used to construct first and second generations (c) of larger icosahedral units according to Hiraga's hierarchical model [18].

Figure 8: Rhombic triacontahedron (a) composed of 10 oblate (b) and 10 prolate (c) rhomhohedra. Second generation cluster of rhombic triacontahedra (d) forming a small segment of a three-dimensional Penrose tiling.

Fiogure 9: Matrix of computer-simulated images for 11 different small cluster models for objective lens defocus - $1000 \leq \Delta f$ Å ≤ 400. Compare different models for Scherzer optimum image condition (Δf = - 600 Å), then compare this with different defoci.

Figure 10: Matrix of computer-simulated images for 7 extended Penrose clusters for objective lens defocus - $1000 \leq \Delta f$ Å ≤ 400. Compare model sensitiveness of images for Scherzer defocus (Δf = - 600 Å) then also compare for deviations in Δf.

Figure 11: Through-focal series of images (-1000 ≤ Δf Å ≤ 400) for model Q for instrtumental resolution in the range 3.5 Å to 1.35 Å. Note increasing detail for the latter, with however no increase in interpretable structural information.

Figure 12: Through-focal series of images (- 1000 ≤ Δf Å ≤ 1400) for (a) centred and (b) non-centred second generation hierarchical clusters. Note model sensitiveness of the images, without, however, any obvious inversion to map out the structure of the cluster (cf. Fig. 7). (c) Shows through-focal-series (- 1000 ≤ Δf Å ≤ 400) of computer-simulated images of the rhombic triacontahedral cluster (cf. Fig. 8). Images are quite distinct from (a) and (b).

TABLE 1:

SUMMARY OF CLUSTER STRUCTURES

Figure Number	Code	Number of Atoms	Cell Dimensions (a x b x c $Å^3$)
3a,b	A	40	11.86 x 11.86 x 4.8
3c,d	B	40	11.86 x 11.86 x 4.8
5a,b	C	95	11.86 x 11.86 x 10.65
5e	D	90	11.86 x 11.86 x 10.65
5f	E	85	11.86 x 11.86 x 10.65
5g	F	80	11.86 x 11.86 x 10.65
5c,d	G	90	11.86 x 11.86 x 9.17
3e,f	H	70	11.86 x 11.86 x 9.17
8c	I	42	34.76 x 34.76 x 16.9
8d	J	202	34.76 x 34.76 x 16.9
7a,c	K	116	11.86 x 11.86 x 13.8
7b,c	L	104	11.86 x 11.86 x 13.8
7c	M	1292	31.05 x 31.05 x 36.50
7c	N	1148	31.05 x 31.05 x 36.50
4a	O	920	55 x 55 x 10.64
6h	P	1052	55 x 55 x 10.64
4b	Q	1080	55 x 55 x 13.30
6d	R	1502	55 x 55 x 15.96
6e	S	1452	55 x 55 x 15.96
6f	T	1356	55 x 55 x 15.96
6g	U	1260	55 x 55 x 15.96

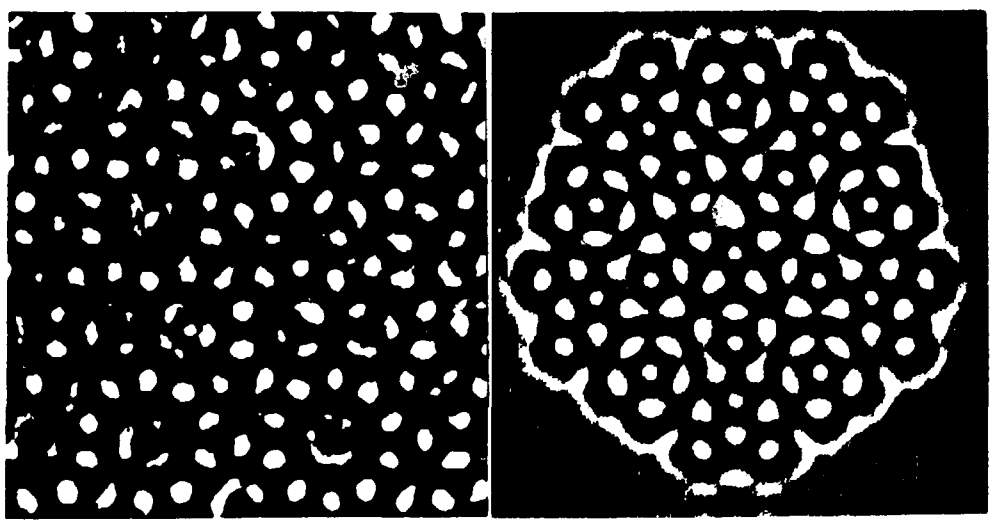

Fig 1

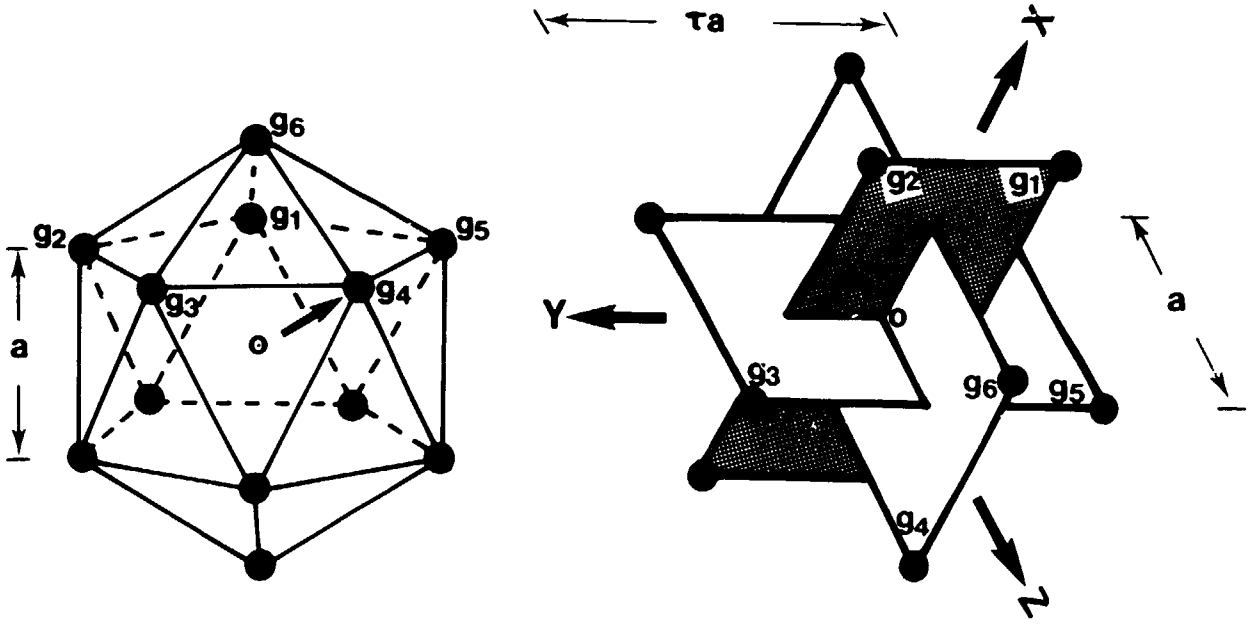

Fig 2

Penrose-Burnell 1979

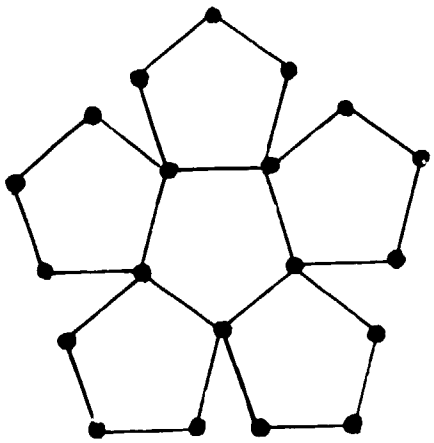

a

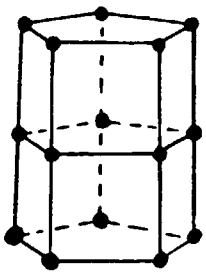

b

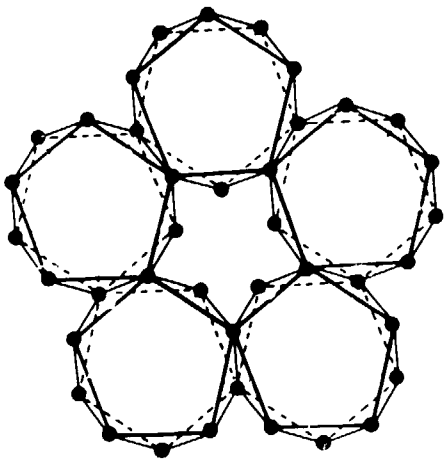

c

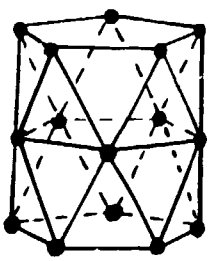

d

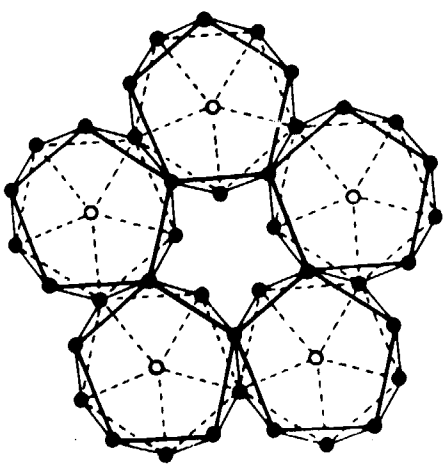

e

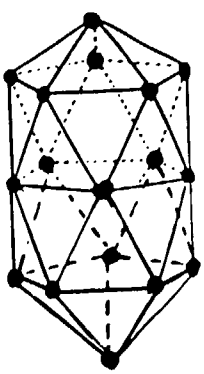

f

Fig 3

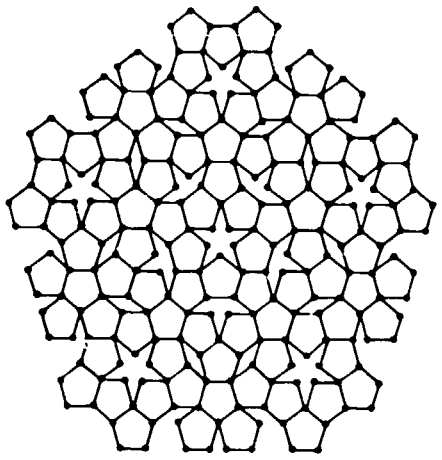

a

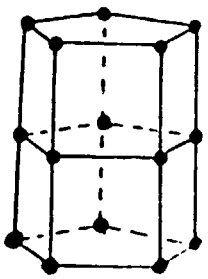

d

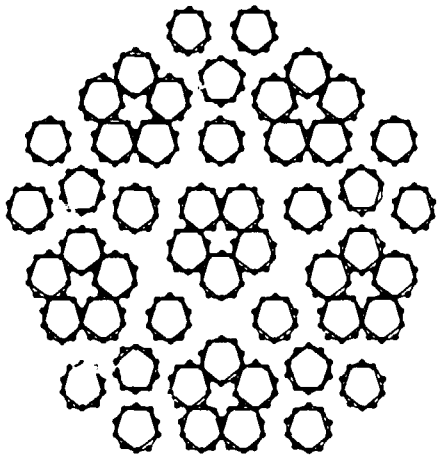

b

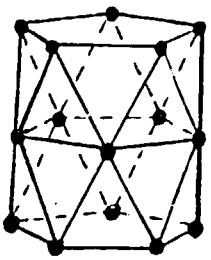

e

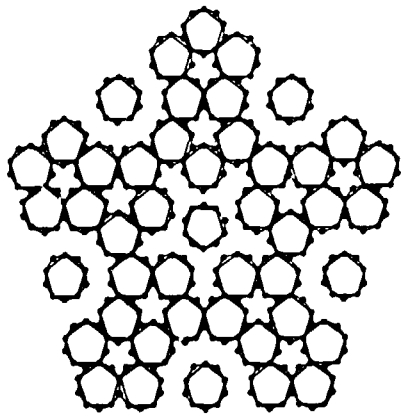

c

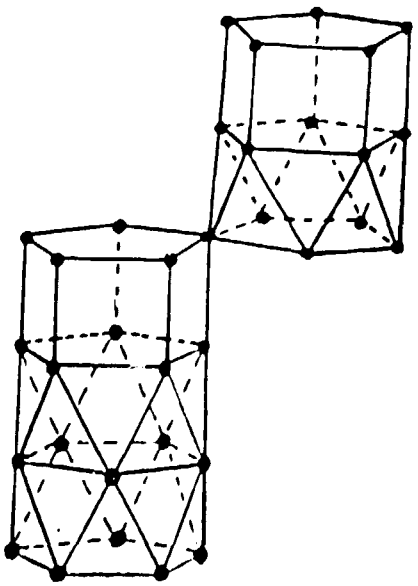

f

Fig 4

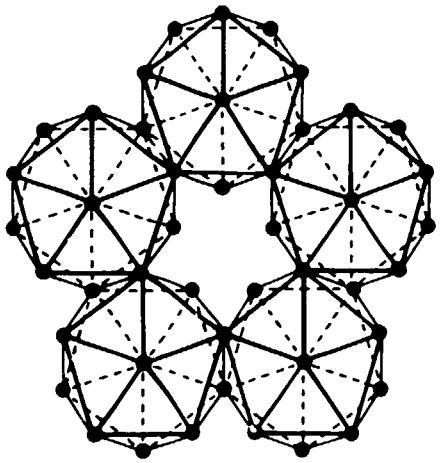

a

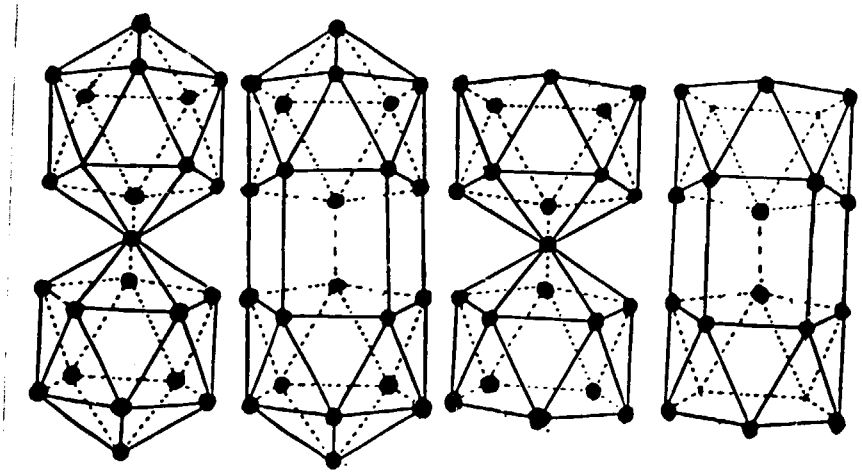

b e f g

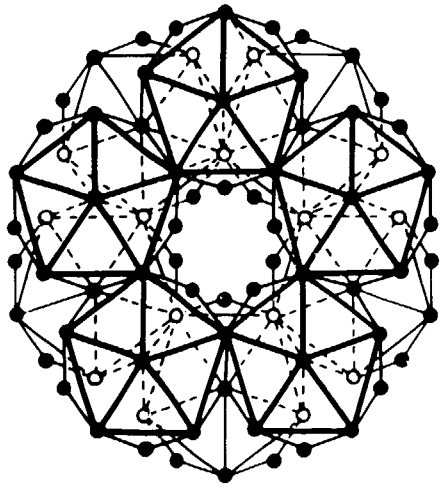

c

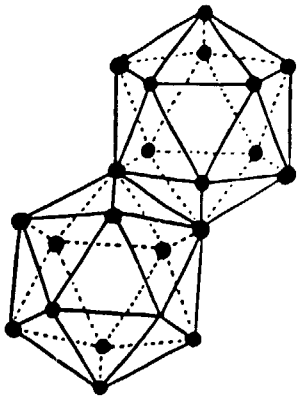

d

Fig 5

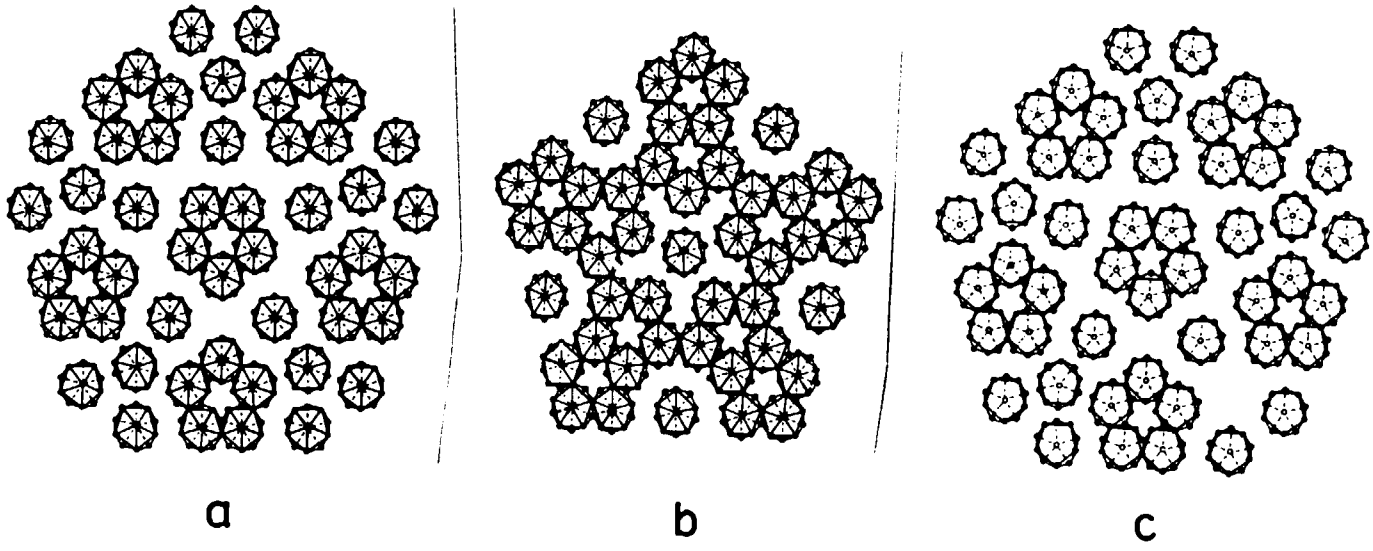

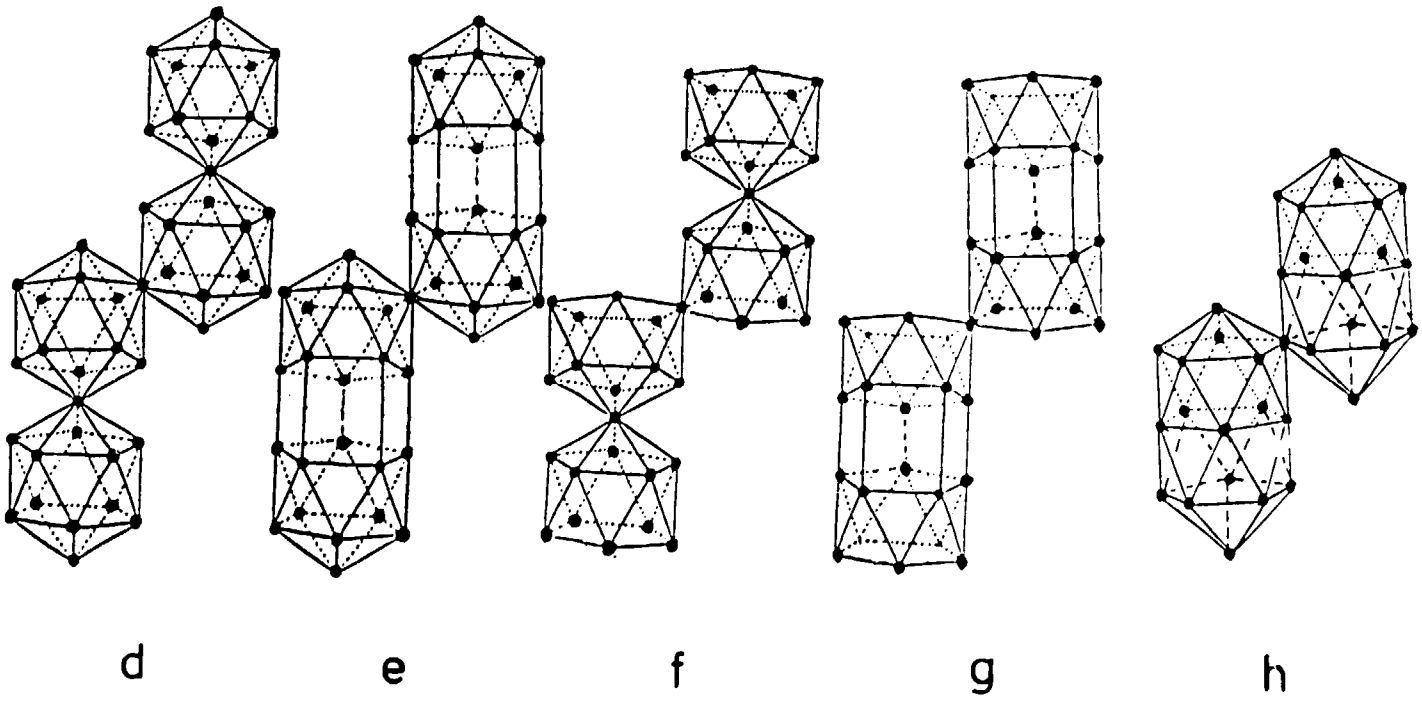

Fig 6

Penrose Bunell 1984

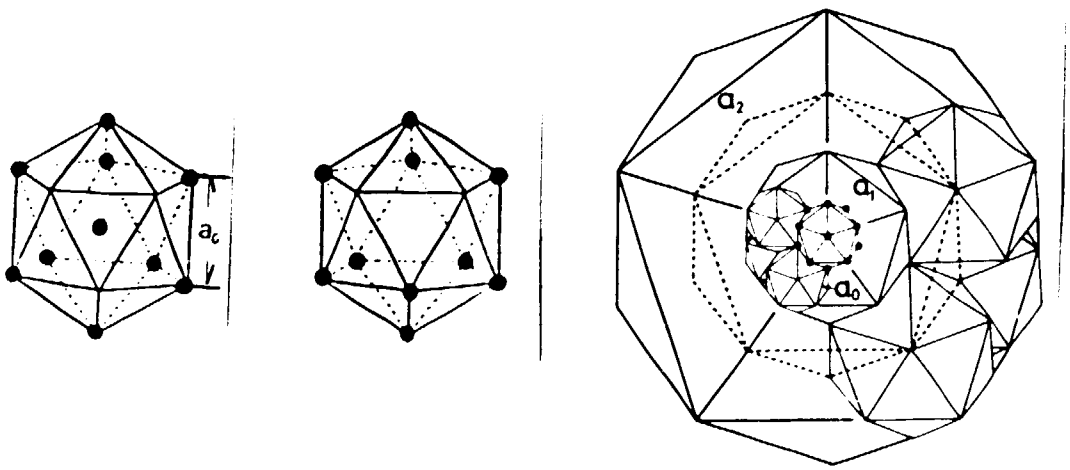

Fig 7

Penrose Bundle 1981

SYMMETRY : quasicrystals

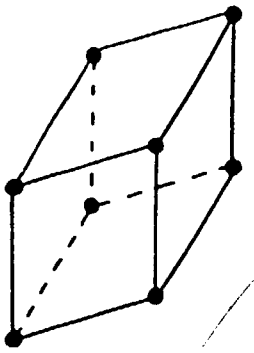

a

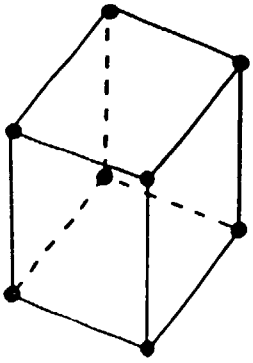

b

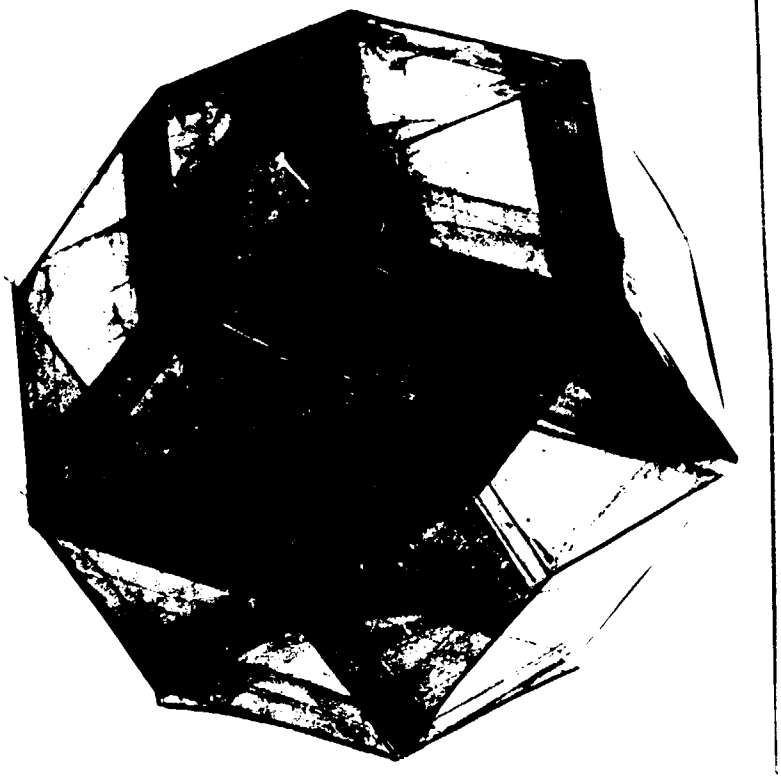

c

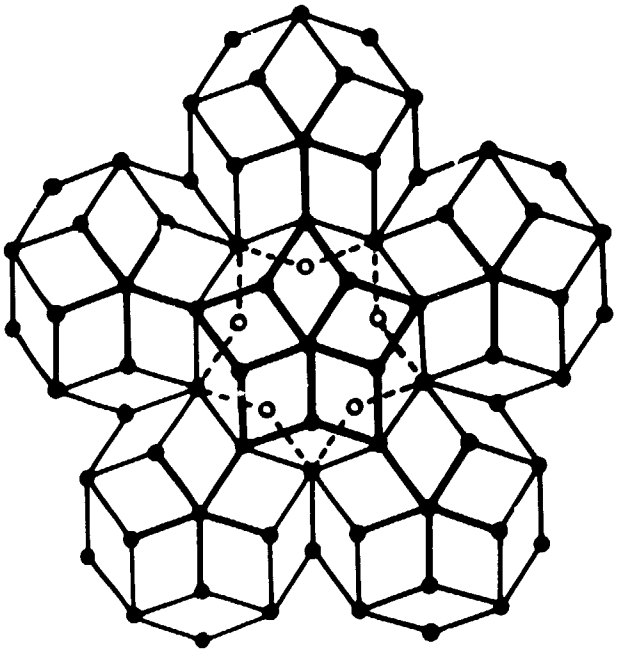

d

Fig 8

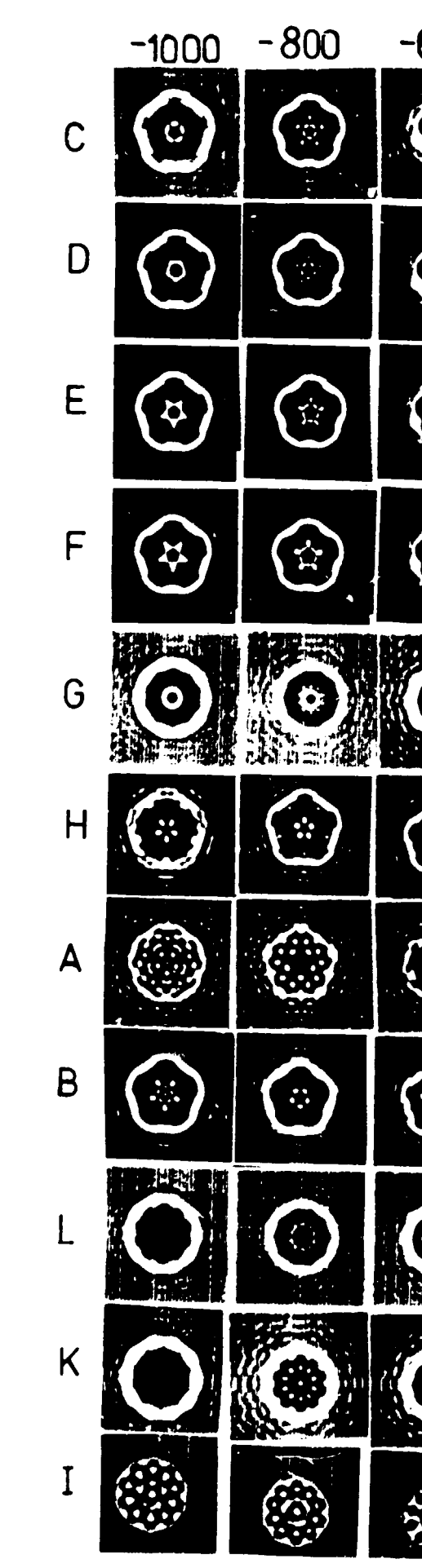
-1000
-800
C
D
E
F
G
H
A
B
L
K
I

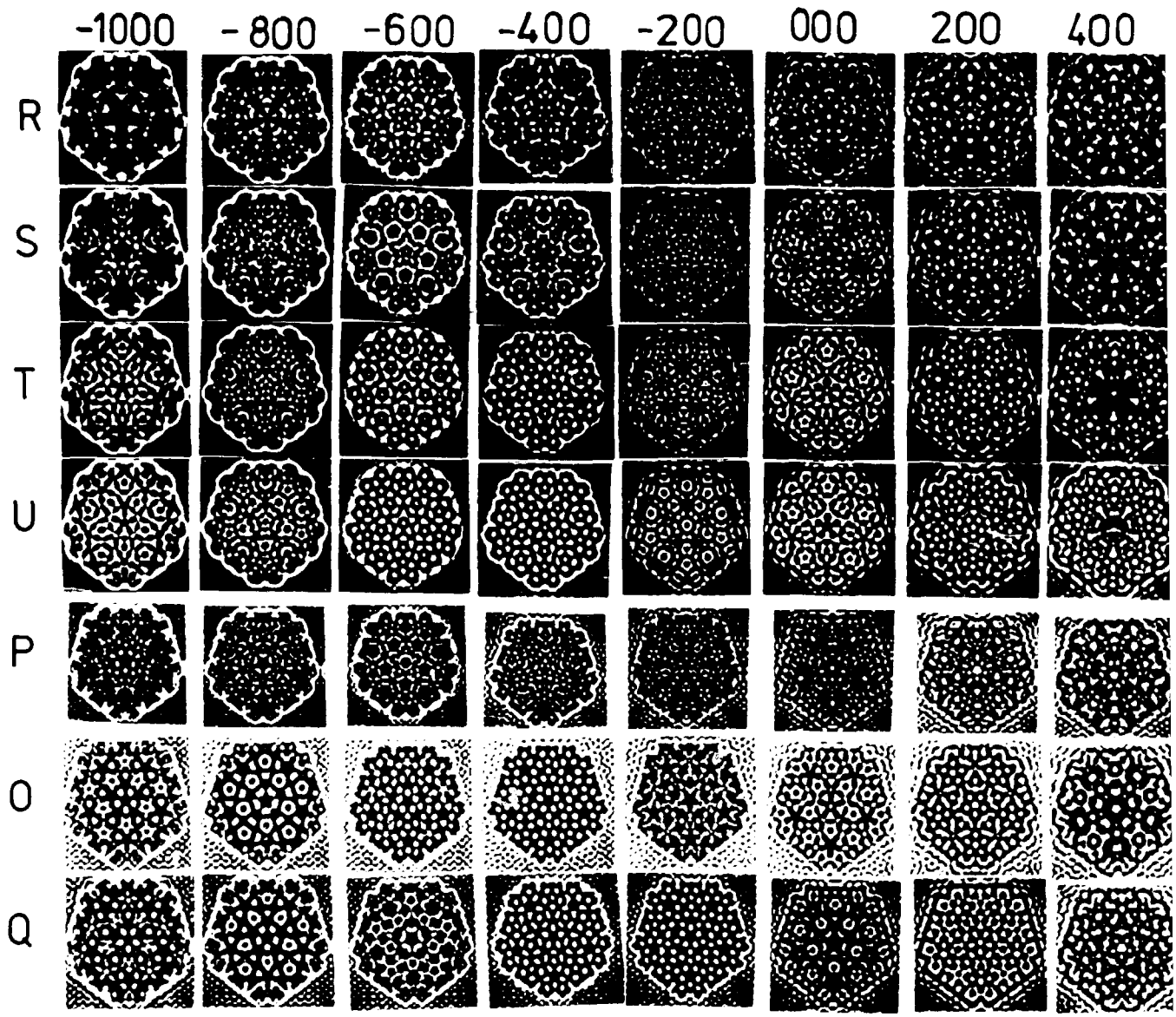

Fig 10

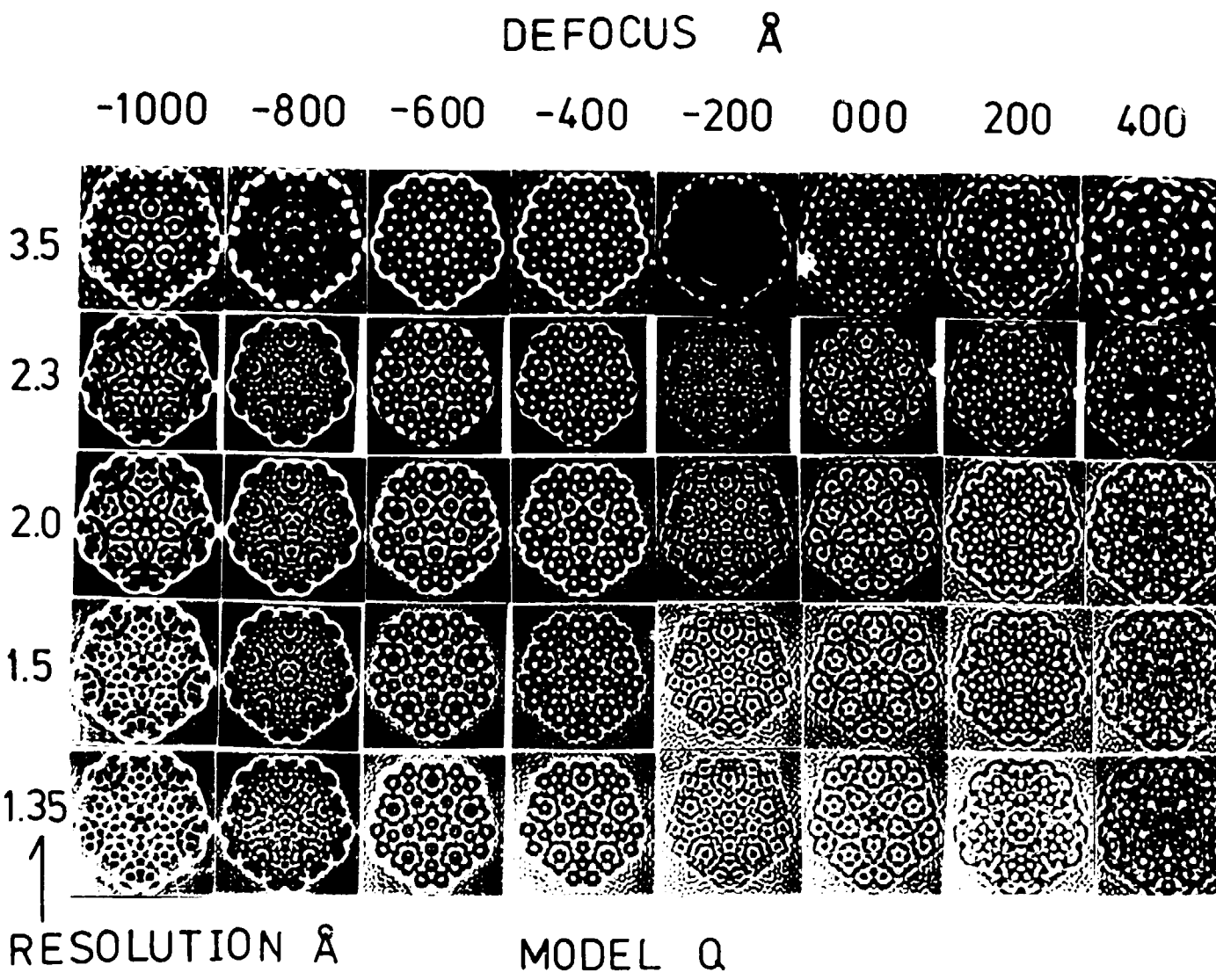
DEFOCUS Å
-1000
-800
-600
-400
-200
000
200
400
3.5
2.3
2.0
1.5
1.35
RESOLUTION Å
MODEL Q

Fig 11

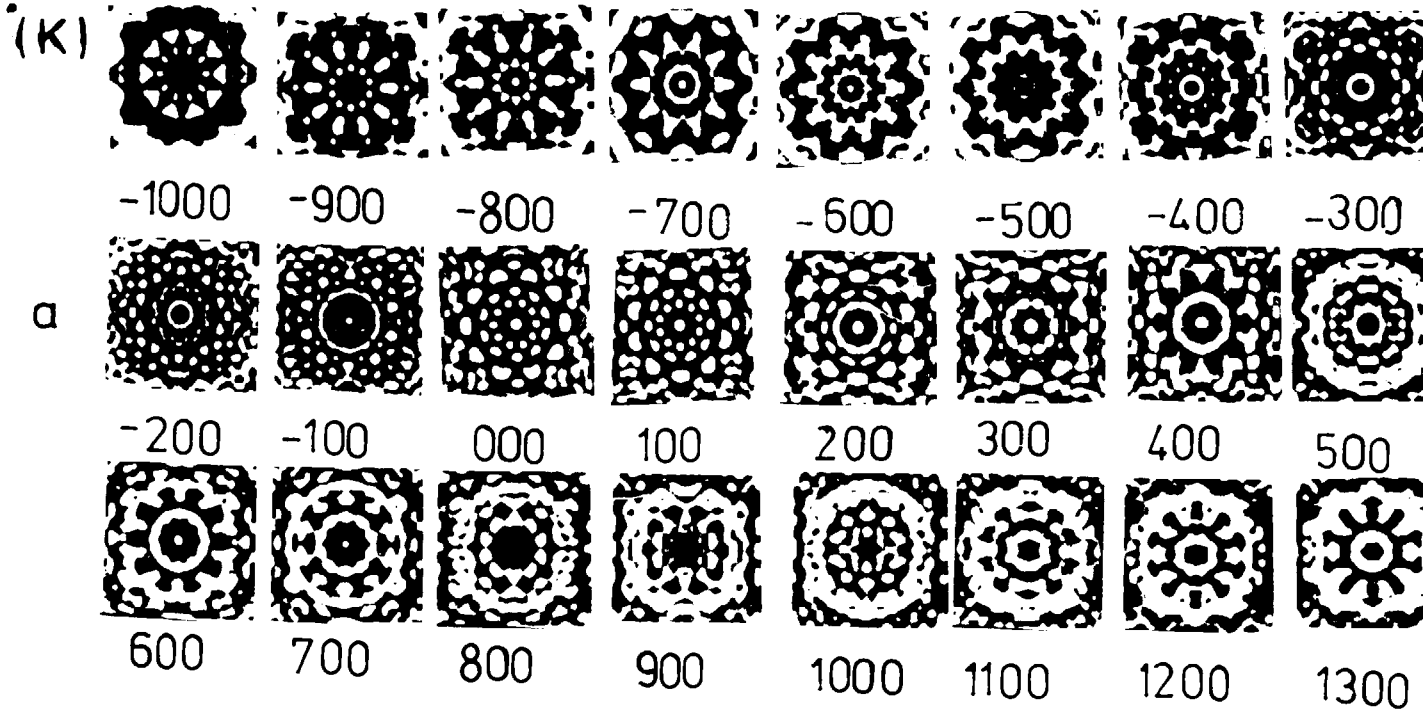
(K)
-1000
-900
-800
-700
-600
-500
-400
-300
a
-200
-100
000
100
200
300
400
500
600
700
800
900
1000
1100
1200
1300
DEFOCUS Å

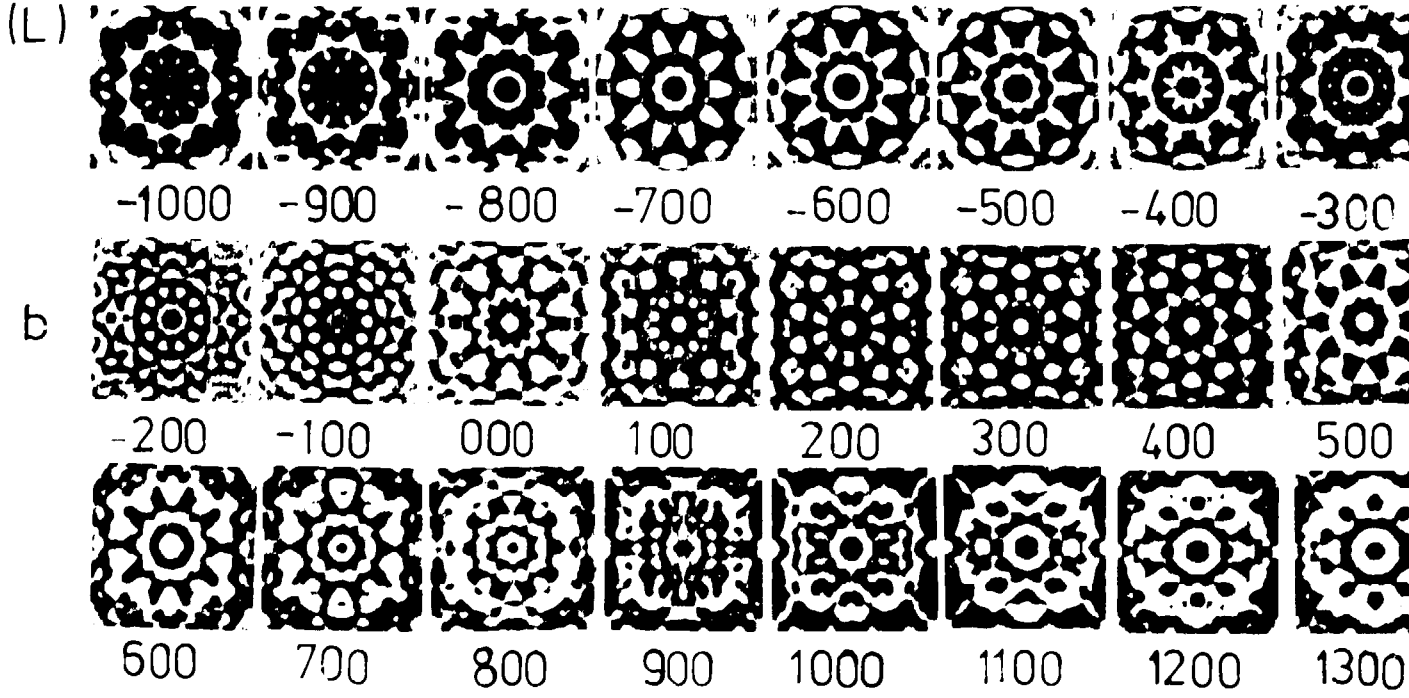
(L)
-1000
-900
-800
-700
-600
-500
-400
-300
b
-200
-100
000
100
200
300
400
500
600
700
800
900
1000
1100
1200
1300


(J)